SIMULATION OF TURBULENT FLOW AROUND TWO CYLINDERS IN TANDEM

G.M. Fishpool, N. Li and M.A. Leschziner
Department of Aeronautics,
Imperial College London
Prince Consort Road
South Kensington
London, UK, SW7 2AZ
geoff.fishpool@ic.ac.uk, n.li@ic.ac.uk and mike.leschziner@ic.ac.uk

ABSTRACT

The physics of the flow around two equal-diameter cylinders in tandem, with centres separated by 5.1 diameters, is discussed by reference to well-resolved large eddy simulations, with initial single-cylinder simulations providing evidence on the adequacy of the computational methodology. The emphasis is on analysing the interaction of the rear cylinder with the turbulent wake of the front cylinder - in particular, the manner by which the rear cylinder deflects and fragments the oncoming large vortices shed from the front cylinder. The study demonstrates, among others, that the shedding from the rear cylinder is locked to that of the front cylinder. Histories of drag, lift, and vorticity flux are considered to illuminate major physical processes. The results demonstrate the importance of sufficient spanwise extent in allowing the 3-dimensional character of the flow to be simulated.

INTRODUCTION

Bluff-body flows are characterised by highly energetic, unsteady, large-scale motions, which include harmonic as well as stochastic components, the former associated with periodic vortex shedding. In these circumstances, statistical flow modelling, even if predicting the time-mean behaviour correctly, is unable to provide essential information on peak forces, unsteady loading, acoustics and fatigue, which are often of primary interest for the design and operation of equipment of which bluff bodies are major components. In contrast, large eddy simulation (LES) offers the required level of detail, at least in principle. However, considerable care is required in its application, especially to multi-body configurations involving separation from curved surfaces. In particular, the resolution near walls, in the separated shear layers and wakes, the positioning of domain boundaries, the conditions prescribed at *free-stream* boundaries, and the nature of the subgrid-stress modelling can all have important consequences for the accuracy with which the physical processes are resolved.

The flow around a single circular cylinder is a generic bluff-body configuration of the above type that has been extensively studied using LES, usually on circular (cylindrical-polar) grids, so as to maximise the accuracy of the method. Many studies of this type are reviewed by Franke and Frank (2002). A key feature of the large majority of simulations for single cylinders is that the approach flow is irrotational and essentially free of turbulence. However, the practitioner is often concerned with incident flows that are sheared and have a high level of turbulence as a consequence of turbulent wakes generated by upstream bodies. The flow around a pair of cylinders, with one subjected to the wake of the other, is a basic configuration involving such an interaction and is thus of both fundamental and practical interest. This arrangement of cylinders is conventionally referred to as *tandem* (Zdravkovich, 1977). When a pair of cylinders in tandem are sufficiently close to each other, there is a strong two-way coupling, one manifestation of which is the absence of the usual vortex shedding from the front cylinder. The separation distance at which periodic shedding from the front cylinder occurs is a function of the Reynolds number, but a centre-to-centre spacing of greater than 4 diameters is normally sufficient for it to arise. At larger distances, the predominant process is one in which the highly unsteady flow of the front cylinder strongly affects the rear one, while the reverse interaction is weak. This is the configuration of interest herein.

This paper presents a computational study of a tandem configuration, with a centre-to-centre spacing of 5.1 diameters, at a Reynolds number of 10,000 (based on the cylinder diameter and the free-stream velocity). These conditions allow direct comparisons to be made with the experimental data of Lin *et al.* (2002). Particular emphasis is given to an analysis of how the large-scale vortices generated by the front cylinder are deflected and fragmented by the rear cylinder, and how this process affects drag, lift and vorticity flux past the rear cylinder.

Preliminary studies have also been undertaken for single cylinders at Reynolds numbers of 3,900 and 10,000, with particular emphasis being placed on the sensitivity to grid distortion. These issues are relevant to the tandem configurations, because significant grid distortions are unavoidable when block-structured meshes are used to map multiple-body geometries.

COMPUTATIONAL APPROACH

Simulations presented below have been performed with an in-house block-structured finite volume procedure reported by Temmerman *et al.* (2003). This uses a co-located-storage scheme combined with a second-order fractional step method for time advancement, second-order spatial discretisation, and multigrid acceleration. Subgrid-scale processes are represented by the dynamic (Germano) version of the Smagorinsky model. The suitability of the code for the current work has been verified by performing simulations for a benchmark case of flow around a single circular cylinder at a Reynolds number $Re = 3,900$ using a cylindrical-polar grid of outside (boundary) diameter $30D$ and spanwise extent, $L_z = \pi D/2$ (where D is the diameter of the cylinder). A second simulation using the same grid, but with Reynolds number increased to 10,000 provides a reference for the principal, tandem-cylinder simulation that is considered later. Finally, a third simulation for the single cylinder at $Re = 3,900$ has been performed on a modular (multiblock) mesh that features substantial distortions, and is of the type and resolution quality of the mesh used later for the tandem cylinders.

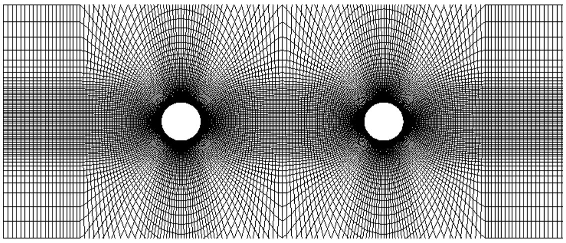

Figure 1: The tandem grid - every other grid line per direction is shown.

The modular grid contains rectangular modules with one corner replaced by a quadrant of a cylinder. Four of these modules combine to produce a block with cross-stream width of $20D$ (where D is the diameter of the cylinder), streamwise length of $5.1D$ and spanwise extent $\pi D/2$. Simple modules of rectilinear grids upstream and downstream of the cylinders give a total distance of $12D$ between the inflow and outflow boundaries and the closest cylinder surface. The central region of the tandem-cylinder grid is outlined in Fig. 1. Each complete plane of this grid has 135,168 cells.

In both circular and modular grids, no-slip and no-penetration boundary conditions are imposed at the surface of the cylinder on a ring of 384 cells with a radial extent of $2 \times 10\ \ ^{3}D$. At the upstream, upper and lower boundaries, the streamwise velocity $u = U_0$ is prescribed, where $U_0 = 1$ is the free-stream velocity. The outflow-boundary condition is of the non-reflecting convective type, and the spanwise-boundary condition complies with periodicity.

Initial simulations with all grids used 24 planes of cells to cover a spanwise extent of $L_z = \pi D/2$. This was chosen based on the results of Kravchenko and Moin (2000), in which this extent was found to allow satisfactory reproduction of single-cylinder near-wake features at $Re = 3,900$. A second grid was also used for tandem-cylinder simulations, with twice the spanwise extent ($L_z = \pi D$) by using 48 planes of cells. The majority of the tandem-cylinder results reported here use the latter grid.

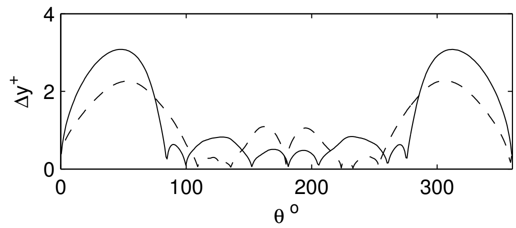

Figure 2: $\Delta y^+(\theta)$ of the wall-nearest layer of nodes around the tandem cylinders; front (solid) and rear (dashed).

The mean-flow results from the simulation with spanwise extent πD are used to assess the chosen near-cylinder grid resolution, in terms of wall units, and this is conveyed in Fig. 2 by means of the radial extent of the wall-nearest cell as a function of angle θ, where θ, measured clockwise from the upstream horizontal centreline of the cylinder. Based on considerations by Piomelli and Chasnov (1995), the desirable near-wall grid parameters are $\Delta y^+ \approx (2y_1^+) < 4$, $\Delta x^+ = 50\ \ 150$, $\Delta z^+ = 15\ \ 40$. With x interpreted here as the circumferential direction and y the radial direction, the modular grid has $\Delta y = 0.002D$, $\Delta x = 0.008D$, $\Delta z = 0.065D$. For the downstream faces of the cylinders, with $\Delta y^+ < 1$, the resolution in all three directions falls well within the above recommended ranges. However, the resolution in the spanwise directions is marginal for the upstream face of the rear cylinder (the flow is laminar over the upstream face of the front cylinder and the spanwise resolution is less important).

Given the high level of distortion in some parts of the modular grid, a check of its adequacy was made by implementing the exact boundary conditions for the inviscid flow around a single cylinder and then computing that flow, subject to zero fluid viscosity and slip conditions at the cylinder wall. A comparison with the exact solution throughout the computational domain showed the error in the total velocity to be lower than $10\ \ ^{3}U_0$, except far from the region of interest, towards the edges of the domain.

All simulations use a variable time step with CFL number ≤ 0.2. Where average values are quoted these are derived from periods with at least 25 vortices shed, after an initial period of settling in which at least 10 vortices have been shed. Increasing the averaging times refines the values at the level of the least significant figures quoted, and the qualitative conclusions discussed here are not affected.

RESULTS: SINGLE CYLINDER

The flow around a single cylinder gives rise to the well-known periodic shedding of large scale vortices[1] forming the *von Karman street*.

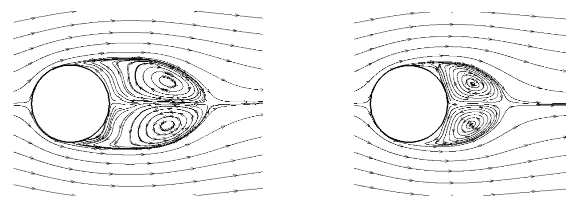

Figure 3: Mean streamlines at $Re = 3,900$ (left), and $Re = 10,000$ (right).

The results of the simulations of the single-cylinder flow, using both the circular and modular grids compare favourably with published experimental and simulation results, e.g. those discussed by Kravchenko and Moin (2000). With the Reynolds number increased to 10,000, the simulated flows are comparable with the experimental results of Lin *et al.* (2002). The computed average values of the Strouhal number, S, drag coefficient, C_D, and negative base-pressure coefficient, $\ \ C_{pb}$ are given in Table 1, and Fig. 3 shows mean streamlines at $Re = 3,900$ and $Re = 10,000$. The differences between the values obtained with the circular and modular grids are not statistically significant, especially in view of uncertainties arising from the need to include the effects of very long time-scale modulation in the flow variables, that are also reported by Breuer (1998) and Franke and Frank (2002).

A detailed comparison of the simulations at $Re = 3,900$ with those of Kravchenko and Moin (2000) shows good agreement, and confirms that the spanwise extent $L_z = \pi D/2$ is acceptable (though not generous) for reproducing the main features of the flow in the near wake. However, the results of the tandem simulations, reported later, show that increasing the spanwise extent to $L_z = \pi D$ makes

[1]The term "vortex" is used hereafter to refer to these large-scale entities.

Table 1: Average values of Strouhal number, S, drag coefficient, C_D, and base-pressure coefficient, C_{pb}, for single cylinder, $L_z = \pi D/2$. Ref. 1 is the $N_z = 24$ case from Kravchenko and Moin (2000), Ref. 2 is Norberg's result reported by Dong *et al.* (2006).

Re	Grid	S	C_D	C_{pb}
3,900	Circular	0.216	1.05	0.99
3,900	Modular	0.214	1.08	1.04
3,900	Ref. 1	0.212	1.07	0.97
10,000	Circular	0.202	1.31	1.41
10,000	Ref. 2	0.201	-	1.11

a significant difference to the results of the simulation at $Re = 10,000$. Therefore, there is reason to expect that the single-cylinder simulation at this higher Reynolds number could also be improved - with the drag expected to drop possibly by about 10% upon doubling the spanwise extent.

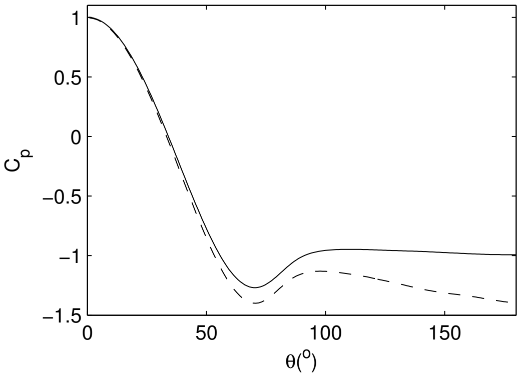

Figure 4: Pressure coefficient around the cylinder at $Re = 3,900$ (solid) and $Re = 10,000$ (dashed).

The circumferential variations of the average pressure coefficient computed at $Re = 3,900$ and $Re = 10,000$ are shown in Fig. 4. The higher minimum pressure at around $\theta = 70°$ for the lower Reynolds number is associated with the longer, more *streamlined* mean flow and with a lower acceleration upstream of separation. However, the dominant contribution to the increased drag at $Re = 10,000$ is from the further decrease in pressure across the base region. At the higher Reynolds number, the vortices form immediately behind the cylinder. As a result, there is a significant velocity magnitude over the rear of the cylinder from the growing vortices. Thus, although this flow oscillates in sign, there is a significant mean dynamic pressure, with a consequent reduction in the mean static pressure.

RESULTS: TANDEM CYLINDER

General Flow Features

For the cylinder spacing and Reynolds number considered, the flow around tandem cylinders exhibits shedding of large-scale, turbulent vortices from both cylinders, as described by Zdravkovich (1977). There is a periodic growth and release of vortices from the front cylinder. These are carried downstream, deform as they pass around the rear cylinder, and then merge with (and thereby trigger the release of) vortices forming from the boundary layers of that cylinder. Throughout their passage, the vortices evolve over

Table 2: Average values of Strouhal number, S, drag coefficient, C_D, and base-pressure coefficient, C_{pb}, for tandem cylinders: front (f), rear (r).

L_z	S	$C_{D,f}$	$C_{D,r}$	$C_{pb,f}$	$C_{pb,r}$
$\pi D/2$	0.185	1.37	0.43	1.51	0.87
πD	0.188	1.22	0.48	1.26	0.76

a wide range of length-scales, becoming highly distorted in all three dimensions.

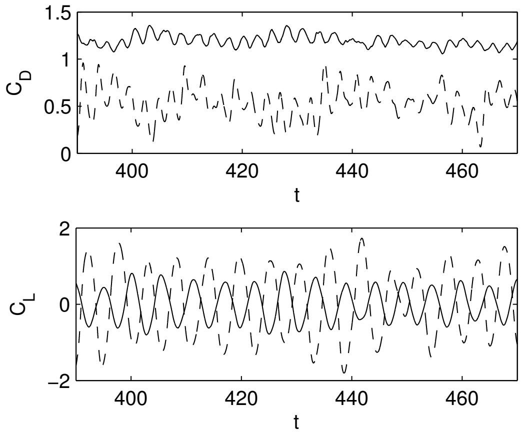

Figure 5: Variation with time of spanwise-averaged C_D and C for front cylinder (solid line) and rear cylinder (dashed line): ($L_z = \pi D$).

The periodic shedding of vortices produces oscillations in the lift and drag coefficients for both cylinders, but the time-histories of the respective coefficients are different, as shown in Fig. 5, in which $t = U_0 t\ /D$ is the non-dimensional time (t is the dimensional value). Average values of the drag and base-pressure coefficients are shown in Table 2. For comparison, the values for the coefficients derived from the simulation with both $L_z = \pi D/2$ and $L_z = \pi D$ are included in the table. Table 2 further shows that the Strouhal number, S, derived from both simulations is in good agreement with the experimental value of 0.185, as reported by Xu and Zhou (2004).

There is a significant difference in the drag on the front cylinder for the two spanwise extents. A more detailed discrimination of this difference is conveyed by the time-mean pressure-coefficient profiles shown in Fig. 6. The profile for the front cylinder agrees well with that for the single cylinder simulated with the same value of $L_z = \pi D/2$. In contrast, the profile for the larger spanwise extent ($L_z = \pi D$) shows a lower acceleration of the flow up to separation, and thereafter a weaker variation across the base region. This difference is qualitatively consistent with the distinction between the single-cylinder simulations at $Re = 3,900$ and $Re = 10,000$.

Kravchenko and Moin (2000) and Ma *et al.* (2000), among others, Demonstrate, for $Re = 3,900$, the importance of a sufficient resolution in the shear layers and vortex-formation region, so as to allow a simulation to correctly represent the physical processes. Cylinder flows at moderate values of Reynolds number (such as herein) are particularly sensitive to resolution, as the transition in the shear layer and subsequent development of turbulence play a key role in determining the mean recirculation length, as discussed by

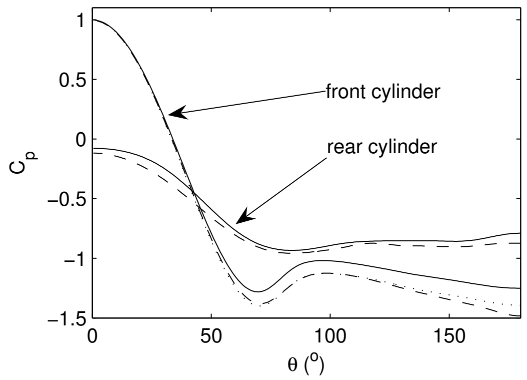

Figure 6: $C_p(\theta)$ for tandem cylinders $L_z = \pi D$ (solid) and $L_z = \pi D/2$ (dashed), with reference single cylinder (dot).

Gerrard (1966). Hence, the implication for the present simulation for $Re = 10,000$ with 24 points in $L_z = \pi D/2$ is that this spanwise resolution does not allow sufficient freedom for physically relevant flow structures to evolve, whereas the larger spanwise extent is significantly less constraining, with the drag and base-pressure of the front cylinder approaching the values of single-cylinder experiments and simulations (Dong *et al.*, 2006).

The strong fluctuations of the rear cylinder drag, seen in Fig. 5, show that longer integration times would be needed in order to determine whether or not the difference in drag on this cylinder between the two simulations is really significant. Fig. 6 suggests that the sensitivity of the front-cylinder drag to the spanwise domain is more pronounced than that of the rear cylinder, although some caution is called for in view of the restricted integration period. This imbalance may be interpreted as reflecting the heightened sensitivity to spanwise resolution of the transition process and structural features in the shear layer separating from the front cylinder and the influence arising therefrom on the flow around the base of that cylinder. A contributory factor may be a subtle, rather weak, effect of the rear cylinder on the front-cylinder wake that requires a high level of resolution.

The total drag on two cylinders with a centre-to-centre separation of $5D$ was reported by Pannell *et al.* in 1915 at a Reynolds number of 9,720, as referenced by Zdravkovich (1977). Pannell *et al.* normalise their measurement by twice the drag on a single cylinder to give a value of ≈ 0.70. Given the drag of the front cylinder as a fair estimate of the drag on a single cylinder, the results from the simulation with $L_z = \pi D$ yield a ratio of 0.70, which is in good agreement with the measurement.

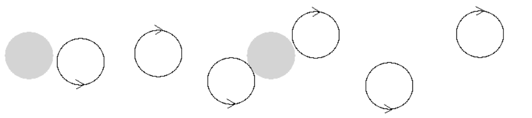

Figure 7: Relative positions of vortices (circulation direction shown) at one phase of the shedding from the two (grey) cylinders.

The lift-coefficient histories in Fig. 5 show that the shedding from the front and rear cylinders is *locked*, and hence Table 2 gives only one Strouhal number for each simulation. This locking is part of the justification for the earlier description of the vortices from the front cylinder triggering the release of vortices from the rear cylinder. The relative locations of a series of successive vortices is illustrated schematically in Fig. 7, for one phase in the cycle, as derived from the simulation (elongation and other shape features are suppressed). The simulated spatial-distribution of the vortices around the rear cylinder agrees with the experiments of Lin *et al.* (2002).

Critical Points in Streakline Topology

The majority of vorticity that is shed into the flow is generated in a pair of boundary layers around the upstream surface of each of the cylinders. The flow around the front cylinder is similar to that around a single cylinder in isolation, and the upper and lower boundary layers are easily identified in Fig. 8, with the base region of the cylinder (to the right) dominated by relatively low-velocity, turbulent motions.

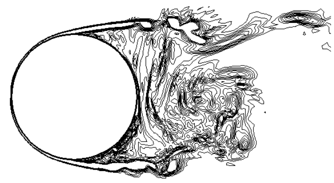

Figure 8: Instantaneous vorticity contours for the front cylinder of the tandem configuration ($L_z = \pi D/2$).

The length of the boundary layers may be represented in terms of the distance from the upstream stagnation point to the separation point. Although the boundary layers on the front cylinder are laminar, these points vary slightly in the spanwise direction, due to instability and turbulent fluctuations further downstream. Hence spanwise-averaged velocities are used to calculate the stagnation and separation locations, and these locations are given in Fig. 9. The figure shows that the shear layers separate a little upstream of $\theta = \ 90°$, the separation angle oscillating with the shedding Frequency and with an amplitude of approximately $3°$. In general, as one separation event moves upstream through the cycle, the one on the opposite side moves downstream, so that the oscillation approximately preserves the total area of attached flow - although there are some longer time-scale variations.

Fig. 9 also shows the upstream stagnation point on the front cylinder oscillating by approximately $2°$, in anti-phase with the separation points. The movement of the stagnation point is a response to the large-scale flow variations, due to the repeated growth and shedding of the vortices, as seen in the lift variation (Fig. 5).

Each vortex that is shed from the front cylinder contains a significant net component of spanwise circulation. As the successive, oppositely-signed, regions of circulation approach the rear cylinder, the initial effect is a periodic deflection of the flow, with the location of the forward stagnation point on the rear cylinder oscillating by as much as $50°$, as shown in Fig. 10. The flow around the rear cylinder features substantial variations in the spanwise direction, and the spanwise-averaged velocity does not reflect well the complex separation behaviour of the boundary layers. However, it is observed that the oscillation of the stagnation point tends to follow the movement of the whole boundary layer. This is indicated, qualitatively, by the contours of instantaneous vorticity for the rear cylinder, shown in Fig. 11. Thus, in contrast to conditions around the front cylinder, the

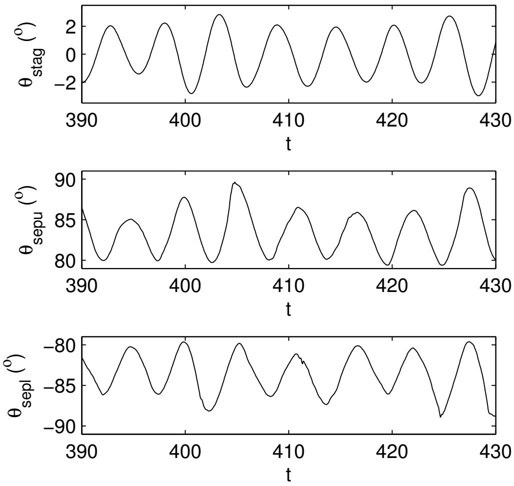

Figure 9: Stagnation ($\theta\ _{ag}$), upper and lower separation points ($\theta\ _{ep}\ ,\ \theta\ _{ep}$) on the front cylinder of the tandem configuration ($L_z = \pi D$).

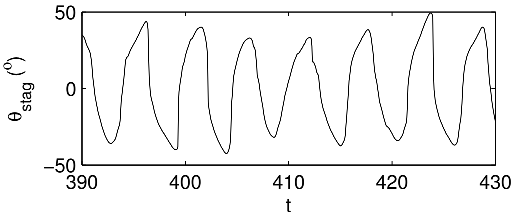

Figure 10: Stagnation ($\theta\ _{ag}$) on rear cylinder ($L_z = \pi D$).

movement of the stagnation point is here broadly in phase with the movement of the separation point, and the stagnation point movement is dominated by the flow upstream of the cylinder, rather than downstream.

Figure 11: Instantaneous vorticity contours for rear cylinder ($L_z = \pi D/2$).

Three-Dimensional Structure

At the present Reynolds number, the fluid motion is highly turbulent, and the resulting spanwise variations are substantial, as is illustrated by a particular snapshop in Fig. 12. The vortices in *side view*, are visualized by surfaces of constant pressure, and the locations of the cylinders are indicated in *plan view* by the circles. Several small vortices due to Kelvin-Helmholtz instabilities in the front-cylinder shear layer are visible.

In Fig. 12, the vortex that is forming on the front cylinder is broadly uniform across the span, the vortex in-between the cylinders displays some distortion, and the vortices around and behind the rear cylinder are highly distorted. However, the distortion is time-dependent, and at another instant in time, the vortex being shed from the front cylinder can be fairly distorted, whilst that being shed from the rear cylinder can be broadly uniform across the span.

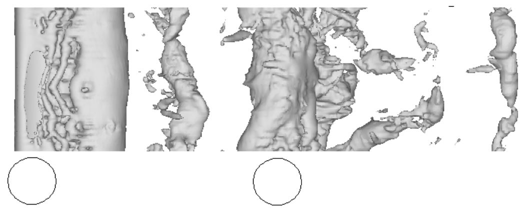

Figure 12: Vortices visualized using pressure isosurfaces.

An example of the detailed structure of the vortices is given in Fig. 13. Contours of spanwise vorticity are shown across an instantaneous slice through the flow field. The phase location is chosen so as to correspond to that of Fig. 7. This illustrates the mixing of regions of oppositely signed circulation.

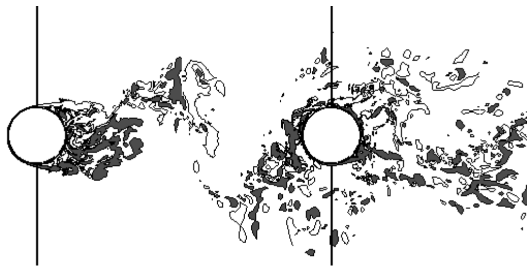

Figure 13: Spanwise vorticity contours $\omega_z = 3$ (filled), $\omega_z =$ 3 (open). Lines show planes across which vorticity flux is analysed.

In what follows, the spanwise-averaged flux (per unit span) of vorticity is determined across chosen planes - to gain insight into the effects of the distortion and mixing of the vortices. The planes chosen are normal to the free stream, passing through the cylinder centre-lines (see vertical lines in Fig. 13). The sign convention means that this flux is (mostly) negative on the upper side of the cylinder, and (mostly) positive on the lower side.

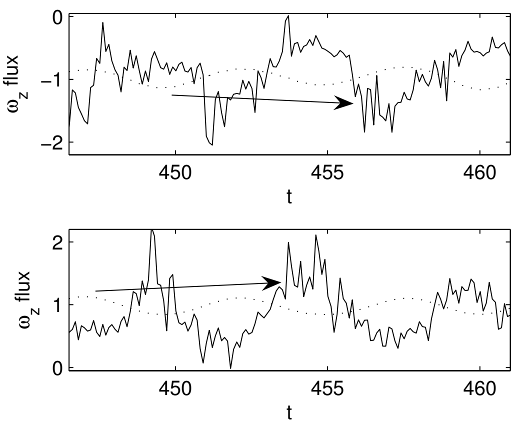

Figure 14: Flux of spanwise vorticity across planes from Fig. 13, front cylinder (dotted lines) and back cylinder (solid lines). Upper/lower plots relate to upper/lower sides of the cylinders. Arrows indicate links between vorticity passing front and rear cylinders.

The lift oscillation on the front cylinder is associated with a relatively simple oscillation in the velocity in the outer regions of the shear layers, the flow velocity in these regions varying between approximately $1.3U_0$ and $1.5U_0$. There is a corresponding oscillation in the flux of vorticity from the shear layer of order 15 %, as seen in the dotted traces of Fig. 14. The maximum magnitude of vorticity flux occurs close to the maximum magnitude of the lift during the growth of the corresponding vortex. The arrows in Fig. 14 indicate the relationship between the flux from which a vortex grows behind the front cylinder and the flux due to that same vortex passing over the rear cylinder.

The vorticity flux past the rear cylinder is comprised of contributions from the boundary layers of that cylinder, and the turbulent vortices coming from the front cylinder. The contribution from the shear layers is similar to that on the front cylinder; though of slightly lower magnitude, due to the mean-momentum deficit of the wake from the upstream cylinder. The erratic nature of the total vorticity flux is the net result of mixed regions of vorticity of both signs (seen in Fig. 13) being convected past. At $t = 447.5$ the flux of positive vorticity from the front-cylinder wake almost completely cancels the flux being shed from the boundary layer of the rear cylinder. The passage of the vortices from upstream alters the velocity at the edge of the shear layer and can cause early separation.

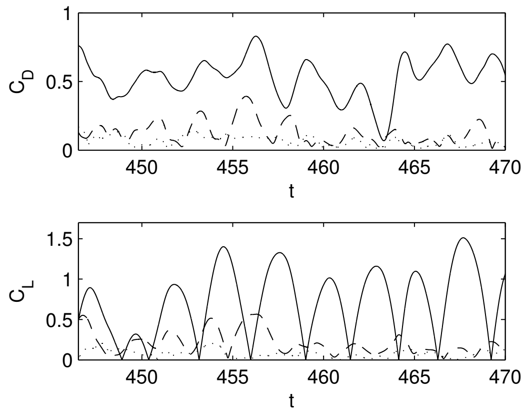

Figure 15: Magnitude of drag and lift coefficient harmonic content for the rear cylinder, $= 0$ (solid), 1 (dashed) and 2 (dotted).

The effect of the flow turbulence on the cylinder forces is seen in Fig. 15. This shows the magnitude of the $= 0$, 1 and 2 harmonics of the drag and lift coefficients for the rear cylinder, where each component has a wavelength of $L_z/$. There are periods during which the spanwise variations are of the same order as the spanwise-average ($= 0$) component, and for the lift around $t = 456$ the dominant component is $= 1$.

CONCLUSIONS

A study has been carried out of the flow around single and tandem cylinders, by means of large eddy simulation, to illuminate, on the one hand, the flow physics involved and to assess, on the other hand, some of the computational issues appertaining to the use of distorted structured meshes in LES around bluff bodies. The procedure employed has been shown capable of simulating satisfactorily a standard test case of flow around a circular cylinder at $Re = 3,900$, both on a well-disposed cylindrical-polar mesh and a distorted modular mesh, the latter of the type subsequently used to compute the flow around the tandem cylinders.

The general characteristics of the flow around tandem cylinders at $Re = 10,000$ and centre-to-centre spacing of 5.1 diameters have been documented and analysed both in comparison with published experimental results, and by contrast with results for a single cylinder at the same Reynolds number. For these conditions, the simulations show that the vortex shedding from the rear cylinder is essentially controlled by (locked to) the vortex shedding from the front one. However, the turbulent evolution of the vortices leads to significant mixing of regions with oppositely signed circulation, and decorrelation in the spanwise direction. This produces fluctuating spanwise-variation in lift and drag coefficients.

The spanwise decorrelation is most significant in the simulation with the largest spanwise extent, $L_z = \pi D$. It seems likely that a further increase in L_z would increase the level of decorrelation, with a consequent reduction in spanwise-averaged lift coefficients. However, the agreement of the simulation with $L_z = \pi D$ with the experimental results suggests that most of the essential physics of the flow around long cylinders in tandem can be captured within a domain of this size.

REFERENCES

Breuer, M., 1998, "Large eddy simulation of the subcritical flow past a circular cylinder: numerical and modeling aspects", *Int. J. Numer. Meth. Fluids*, Vol. 28, pp. 1281-1302.

Dong, S., Karniadakis, G.E., Ekmekci, A., and Rockwell, D., 2006, "A combined direct numerical simulation-particle image velocimetry study of the turbulent near wake", *J. Fluid Mech.* Vol. 569, pp. 185-207.

Franke, J., and Frank, W., 2002, "Large Eddy Simulation of the Flow Past a Circular Cylinder at $Re_D = 3900$", *J. Wind Eng. Ind. Aerodyn.*, Vol. 90, pp. 1191-1206.

Gerrard, J.H., 1966, "The mechanics of the formation region of vortices behind bluff bodies", *J. Fluid Mech.* Vol. 25, pp. 401-413.

Kravchenko, A.G., and Moin, P., 2000, "Numerical studies of flow over a circular cylinder at $Re_D = 3900$", *Phys. Fluids*, Vol. 12 (2), pp. 403-417.

Lin., J.-C., Yang, Y, and Rockwell, D., 2002, "Flow past two cylinders in tandem: instantaneous and averaged flow structure", *Journal of Fluids and Structures*, Vol. 16, pp. 1059-1071.

Ma, X., Karamanos, G.-S., and Karniadakis, G.E., 2000, "Dynamics and low-dimensionality of a turbulent wake", *J. Fluid Mech.*, Vol. 410, pp. 29-65.

Piomelli, U., and Chasnov, J.P., 1995, "Large-eddy simulations: theory and applications", In *Turbulence and Transisition Modelling*, Edited by Hallbäck, M., *et al.*, Kluwer Academic Publishers, Dordrecht.

Temmerman, L., Leschziner, M.A., Mellen, C.P. and Fröhlich, J. (2003), "Investigation of subgrid-scale models and wall-functions approximations in Large Eddy Simulation of separated flow in a streamwise periodic channel constriction", *Int. J. Heat and Fluid Flow*, Vol. 24, pp. 157-180.

Xu, G., Zhou, Y., 2004, "Strouhal numbers in the wake of two inline cylinders", *Experiments in Fluids*, Vol. 37, pp. 248-256.

Zdravkovich, M.M., 1977, "Review of flow interference between two circular cylinders in Various Arrangements", *Trans ASME J. Fluids Engng* Vol. 99, pp. 618-633.